

Parimagnetism in $R\text{Co}_2$ series ($R=\text{Dy}$, Ho , and Tm)

C. M. Bonilla*

*Instituto de Ciencia de Materiales de Aragón and Departamento de Física de la Materia Condensada,
CSIC - Universidad de Zaragoza, Pedro Cerbuna 12, E-50009 Zaragoza, Spain*

J. Herrero-Albillos

*Fundación ARAID, Paseo María Agustín 36, E-50004 Zaragoza, Spain
Centro Universitario de la Defensa, Ctra. de Huesca s/n, E-50090 Zaragoza, Spain and*

Instituto de Ciencia de Materiales de Aragón, CSIC - Universidad de Zaragoza, Pedro Cerbuna 12, E-50009 Zaragoza, Spain

A. I. Figueroa, C. Castán-Guerrero, and J. Bartolomé

*Instituto de Ciencia de Materiales de Aragón and Departamento de Física de la Materia Condensada,
CSIC - Universidad de Zaragoza, Pedro Cerbuna 12, 50009 Zaragoza, Spain*

I. Calvo-Almazán

*Institute Laue Langevin, 38042, Grenoble, France and
Instituto de Ciencia de Materiales de Aragón and Departamento de Física de la Materia Condensada,
CSIC - Universidad de Zaragoza, Pedro Cerbuna 12, 50009 Zaragoza, Spain*

D. Schmitz and E. Weschke

*Helmholtz-Zentrum Berlin für Materialien und Energie GmbH,
Albert-Einstein-Str. 15, 12489 Berlin, Germany*

L. M. García and F. Bartolomé

*Instituto de Ciencia de Materiales de Aragón and Departamento de Física de la Materia Condensada,
CSIC-Universidad de Zaragoza, Pedro Cerbuna 12, 50009 Zaragoza, Spain*

(Dated: April 2, 2019)

X-ray circular magnetic dichroism (XMCD), longitudinal (χ_{ac}) and transverse (TS) ac magnetic susceptibility have been measured in several members of the $R\text{Co}_2$ series ($R = \text{Dy}$, Ho , and Tm) as a function of temperature and applied magnetic field. We show that parimagnetism is a general behavior along the $R\text{Co}_2$ ferrimagnetic series (R being a heavy rare earth ion). XMCD results evidence the presence of two compensation temperatures, defining two different parimagnetic configurations, which is a fully unexpected result. The inverse χ_{ac} curve exhibits a deviation from Curie-Weiss behavior which is recovered under applied magnetic field. The large excess of polarizability above the critical temperature proves the existence of an enhanced effective moment due to the presence of short range magnetic correlations, which are also observed in TS measurements. The combination of TS and XMCD measurements allows to depict new magnetic phase diagrams for the $R\text{Co}_2$ series. A new scenario allowing to understand the observed phenomenology as a Griffiths phase-like behavior is proposed, where the amorphous $R\text{Co}_2$ represents the undiluted system case.

PACS numbers: 81.30.Bx, 71.20.Lp, 75.20.Hr

I. INTRODUCTION

Among the newly discovered phenomena related to short-range magnetic correlations, an interesting example is the parimagnetic phase observed in ErCo_2 .¹ Parimagnetism consists in the antiparallel alignment of the net magnetization of each sublattice in the magnetically disordered, high temperature phase ($T > T_c$), of a two-sublattice system under an applied magnetic field, differently to the usual paramagnetic phase where the two sublattices would present net magnetizations parallel to the applied magnetic field. This phenomenon indeed contradicts the usual interpretation of the $R\text{Co}_2$ series as simple exchange-enhanced paramagnets with a rare-earth dominated magnetism.²⁻⁴

The hierarchy of exchange magnetic interactions in

$R\text{Co}_2$ is $J_{\text{Co-Co}} \gg J_{\text{R-Co}}$,^{5,6} while $J_{\text{R-R}}$ is usually neglected. Therefore, the formation of Co short-range magnetic correlations in the paramagnetic phase is energetically favored. Indeed, Co magnetic correlations have been previously identified at the origin of some anomalies in the transport properties of $R\text{Co}_2$, but it had been ascribed to critical fluctuations,⁷ near the Curie temperature. Nevertheless, previous works on ErCo_2 and HoCo_2 ; including small angle neutron scattering (SANS),^{1,8} longitudinal (χ_{ac})⁹ and transverse (TS)^{8,10} magnetic susceptibilities and muon spin relaxation spectroscopy (μSR),¹¹ among others, have shown the presence of magnetic correlations not only near T_c , but also at much higher temperatures. Magnetic correlations at temperatures above the ferrimagnetic ordering in ErCo_2 had also been identified in the neutron diffraction pattern^{12,13} and in electri-

cal resistivity measurements.¹⁴ Magnetization and transport properties show the fingerprint of high temperature magnetic correlations in related compounds, such as $\text{Er}(\text{Co}_x\text{Ni}_{1-x})_2$ ¹⁵ and $\text{Er}(\text{Co}_x\text{Ti}_{1-x})_2$.¹⁶ Other intermetallic Laves phases do also show magnetic correlations at high temperatures compared with T_C : Déportes and coworkers¹⁷ claimed the existence of short-range magnetic order at four times T_C in CeFe_2 , evidencing the importance of transition metal interactions in the paramagnetic phase of these intermetallic compounds.

Previous work in ErCo_2 allowed to identify a Griffiths - like phase within its magnetically disordered phase.⁹ A Griffiths phase can be seen as the realization of short-range order, within a diluted magnet of a given concentration x , lying between the percolation concentration, x_p , and the undiluted “pure” system, $x = 1$.¹⁸ The Griffiths phase appears below a given temperature, T_G , above the critical ordering temperature of the diluted system and that of the pure one: $T_c^x < T_G < T_c^1$. The short range order is a kind of low-temperature remnant of the magnetic order of the undiluted system, in the temperature range at which the system would order spontaneously if it were not diluted. This is the scenario in most of the physical realizations of Griffiths phases claimed up to now, as in germanates^{19–22}, manganites^{23–25} and alloys.^{9,22,26,27} The ac-susceptibility curve obtained for ErCo_2 shows the usual deviation from a Curie Weiss behavior below a certain temperature which is, however, recovered under applied magnetic field.^{19,20,22,24} Such extreme sensitivity to the applied field is characteristic of a Griffiths phase.^{23,25} However, the physical origin of a Griffiths - like phase in a pure compound like ErCo_2 is not easy to understand.

From previous experimental work^{1,8–11,28–31} parimagnetism in ErCo_2 is a consequence of short-range correlations between Co magnetic moments and it is natural to investigate whether this phenomenon is present among other ferrimagnetic $R\text{Co}_2$.

A systematic X-ray magnetic circular dichroism (XMCD) study together with magnetic susceptibility measurements performed in $R\text{Co}_2$ with $R = \text{Dy}, \text{Ho}$ and Tm , are presented in order to obtain a more complete description of the magnetism above T_c in these compounds. Our work indicates that parimagnetism observed in the ErCo_2 system is found in the $R\text{Co}_2$ $R = \text{Dy}, \text{Ho}$ and Tm , members of the series too, and the effect of short-range correlations are even stronger than those found in ErCo_2 , showing some unexpected features reminiscent of compensation points in rare-earth transition metal compounds.

II. SAMPLE CHARACTERIZATION AND EXPERIMENTAL DETAILS

Polycrystalline ingots of $R\text{Co}_2$ with $R = \text{Dy}, \text{Ho}$ and Tm were prepared following a standard procedure by melting together the metallic precursors in an arc fur-

nace under Ar atmosphere. An excess of 1% of rare earth has been added to obtain a final sample with the correct stoichiometry, taking into account the amount of rare earth which is evaporated during the melting process. The samples were annealed under Ar atmosphere at 850 °C for twelve days in order to improve the homogeneity. X-ray diffraction analysis on powdered samples was performed in a Rigaku RTO 500RC diffractometer with Bragg-Brentano geometry using $\text{K}\alpha$ Cu radiation at room temperature. The Rietveld analysis shows very well crystallized samples, as shown in previous works¹ and no impurities within the 2% of accuracy of powder diffraction methods.

A complete magnetic characterization has been performed on the powdered samples. The longitudinal ac susceptibility has been measured under applied fields up to $\mu_0 H = 5$ T in a SQUID Quantum Design magnetometer from $T = 4$ K to $T = 400$ K. Magnetization (M) (Fig. 1) and ac susceptibility χ_{ac} as function of temperature measured for the three ferrimagnetic systems show critical temperatures $T_c = 136$ K, 78 K and 4.6 K for DyCo_2 , HoCo_2 , and TmCo_2 , respectively, which coincide with those reported in the literature.³²

The presence of short-range magnetic correlations above T_c has been studied by means of transverse susceptibility (TS). These measurements were performed using a radiofrequency (RF) self-resonant circuit oscillator using CMOS transistors coupled with a LC tank, operating at a frequency of about 12 MHz.³³ The sample and coil set are designed to fit into a commercial Quantum Design PPMS probe such that the perturbing RF magnetic field inside the coil ($\approx 10^{-3}$ T) is oriented perpendicular to the external dc magnetic field H_{dc} supplied by the PPMS superconducting magnet, thus setting the transverse geometry. In a TS measurement at a fixed temperature, the resonant frequency f is recorded as the H_{dc} field is swept from positive to negative saturation (unipolar scan) and then back to positive (bipolar scan). Since the change in frequency of the circuit, Δf , is a direct consequence of the change in inductance as the sample is magnetized, Δf is proportional to the variation of the transverse susceptibility of the sample, $\Delta\chi_T$, the magnitude of physical interest. In the present study, the quantity $[\Delta\chi_T/\chi_T]\% = [\chi_T(H_{dc}) - \chi_T^{sat}]/\chi_T^{sat} \times 100\%$ as function of the applied field H_{dc} is the one considered, where χ_T^{sat} is the transverse susceptibility at the saturating field $\mu_0 H^{sat} = 1$ T, within a temperature range $2.5 \text{ K} < T < 300 \text{ K}$. Details on the technique and the circuit can be found in Ref. 33.

The skin depth, δ , of the $R\text{Co}_2$ compounds has been calculated by the well-known formula $\delta = \sqrt{\rho/2\pi f\mu}$ where ρ is the resistivity, μ the magnetic permeability and f the excitation frequency. The values range between 30 μm at low temperatures and 180 μm for $T > T_c$ up to room temperature. In order to assure that the RF magnetic field penetrates the entire grain the sample has been powdered to reach a grain size of average diameter $\sim 1.5 \mu\text{m}$, well below δ , to avoid the formation of eddy

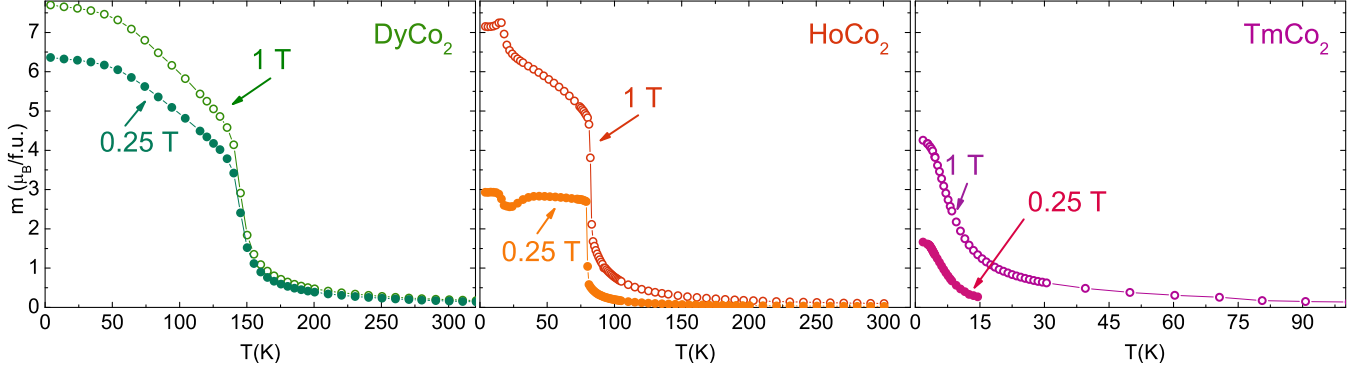


FIG. 1. (Color online) Magnetization as function of temperature at $\mu_0 H = 0.25$ T (full symbol) and $\mu_0 H = 1$ T (open symbol). From left to right for ferrimagnetic systems DyCo_2 , HoCo_2 and TmCo_2 .

currents on the surface.

X-ray absorption spectroscopy (XAS) and X-ray magnetic circular dichroism (XMCD) measurements were carried out at the UE46-PGM1 beamline, at BESSY synchrotron facility, Berlin. The measurements were performed at the Co $L_{2,3}$ and the Dy, Ho and Tm $M_{4,5}$ absorption edges with a polarization rate of 0.9. The temperature was varied between 5 K to 350 K under applied fields between $\mu_0 H = 0.25$ T and $\mu_0 H = 6$ T. The detection method used was total electron yield. In order to prevent the spurious signals due to surface oxidation, the polycrystalline ingots were cleaved in an ultra high vacuum chamber just before starting its exposure to the X-ray beam.

III. EXPERIMENTAL RESULTS

A. X-ray magnetic circular dichroism

DyCo_2 , HoCo_2 and TmCo_2 have been studied by means of XMCD spectroscopy to obtain the element-specific magnetization in these materials. The XMCD signals show the usual spectral shape, for Co $L_{2,3}$ and R $M_{4,5}$ edges, as is mentioned in Refs. 34 and 35 respectively. The XMCD signals at the R M_4 edges have in every case the same sign and (as expected) much reduced intensity with respect to the the R M_5 edge ones, and will be, therefore, omitted in the majority of this work, for the sake of clarity. Figs. 2, 3 and 4 show XMCD spectra for Co $L_{2,3}$ edges (left) and Dy, Ho and Tm M_5 edges (right), respectively, at selected temperatures and at an applied magnetic field of $\mu_0 H = 1$ T for DyCo_2 and TmCo_2 and $\mu_0 H = 2$ T for HoCo_2 .

The Co absorption at the $L_{2,3}$ edges has been normalized using the usual 2:1 branching ratio.³⁶ The normalization of the $M_{4,5}$, has been performed by setting to 1 the maximum of the unpolarized absorption (obtained by averaging right and left polarized light XAS). The net magnetic moment of the rare-earth sublattice has been

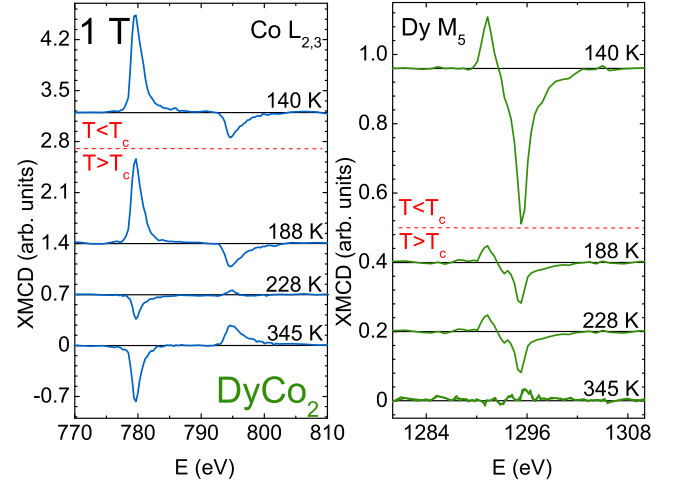


FIG. 2. (Color online) XMCD spectra at the Co $L_{2,3}$ (left) and Dy M_5 (right) edges in DyCo_2 for selected temperatures at $\mu_0 H = 1$ T. Dashed line separates the XMCD spectra measured above and below T_c .

assumed to be proportional to the area under the XMCD signal at R M_5 edge,³⁷ in such a way that negative values for the integral calculated from the XMCD spectrum correspond to a positive sign of the R net magnetic moment. On the other hand, given A and B , the areas under the Co XMCD curves at the L_3 and L_2 edges respectively, the magnetic moment per Co atom is proportional to $-5A + 4B$.³⁴ The spectra at the top of each panel in Fig. 2 and 3, show the XMCD signals recorded below T_c in DyCo_2 and HoCo_2 , respectively. The sign of these spectra demonstrates the ferrimagnetic ordering of these phases, with the larger rare-earth net magnetic moment parallel to the applied field and the Co one, much smaller, antiparallel to it. XMCD could not be measured below T_c on TmCo_2 , as T_c lies below the lowest temperature achievable at the experimental setup.

The temperature range in which a paramagnetic con-

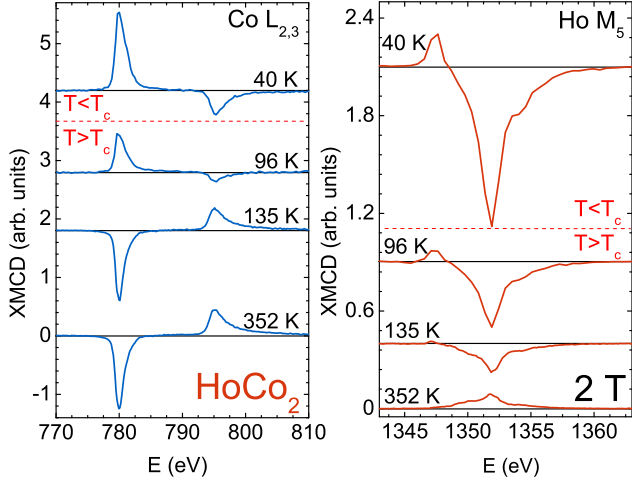


FIG. 3. (Color online) XMCD spectra at the Co $L_{2,3}$ (left) and Ho M_5 (right) edges in HoCo_2 for selected temperatures at $\mu_0 H = 2$ T. Dashed line separates the XMCD spectra measured above and below T_c .

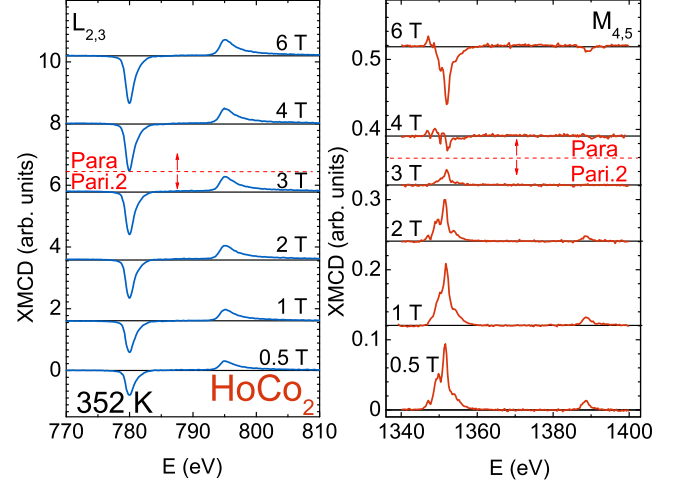


FIG. 5. (Color online) XMCD spectra at the Co $L_{2,3}$ (left) and Ho $M_{4,5}$ (right) edges in HoCo_2 for selected fields at $T = 352$ K. Dashed line separates the paramagnetic and paramagnetic-2 configurations.

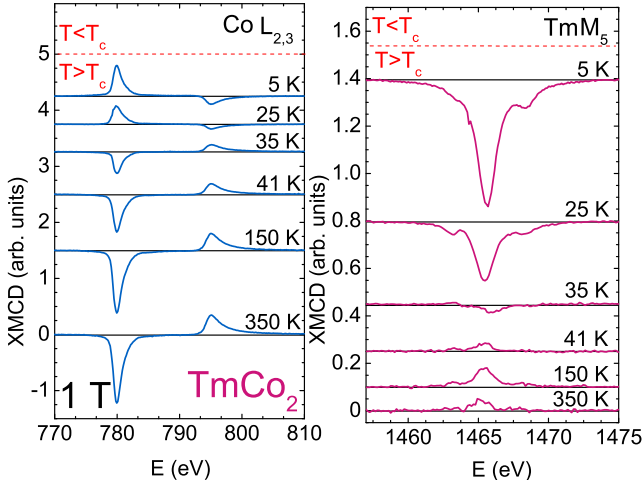


FIG. 4. (Color online) XMCD spectra at the Co $L_{2,3}$ (left) and Tm M_5 (right) edges in TmCo_2 for selected temperatures at $\mu_0 H = 1$ T. Dashed line separates the spectra measured above and below the critical temperature.

figuration takes place on DyCo_2 , can be identified from mere inspection of Fig. 2. Indeed, it is clear that the XMCD signal at the Co $L_{2,3}$ and Dy M_5 absorption edges at $T = 188$ K, ($=T_c + 43$ K at $\mu_0 H = 1$ T) has the same sign as the one recorded at $T = 140$ K, (5 K $< T_c$ at $\mu_0 H = 1$ T). This indicates that on average, the Co and the Dy net moments are antiparallel within a wide range of temperature above T_c . As evidenced in Fig. 2, for applied field $\mu_0 H = 1$ T and $T > 188$ K, the XMCD signal at the Co $L_{2,3}$ changes sign, remaining thereafter unchanged up to the highest studied temperature.

Above the temperature at which the net moment of Co

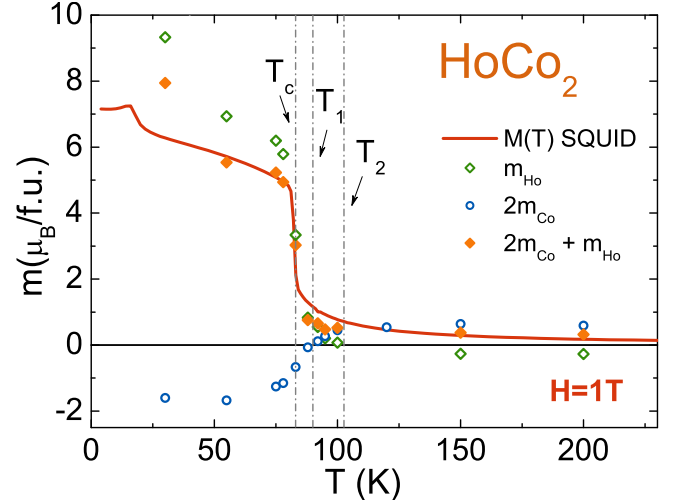


FIG. 6. (Color online) Magnetic moment in HoCo_2 (left) as a function of temperature obtained from the XMCD data treatment. Open circles (\circ) and open diamonds (\diamond) are the net magnetization per atom for Co and rare-earth respectively, while full diamonds \blacklozenge are the sum of the rare-earth and Co magnetization. The continuous line is the SQUID magnetization measurement. T_c is the long-range magnetic ordering temperature, T_1 is the temperature at which the net magnetization of Co changes from negative to positive and T_2 is the temperature at which the net magnetization of the rare-earth sublattice changes from positive to negative.

magnetization sublattice is zero, $T \approx 220$ K, the disordered Co atomic magnetic moments are polarized by the applied magnetic field, creating a positive Co magnetic moment.

Analogous results are obtained in HoCo_2 and TmCo_2 (Fig. 3 and Fig. 4). Well above T_c , at 96 K and 25 K for

HoCo₂ and TmCo₂ respectively, the sign of XMCD signal for Co L_{2,3} edge remains unchanged with respect to the ferrimagnetic phase, which is the telltale characteristic of paramagnetism. At a higher temperature, which depends on the magnitude of the applied field and R , the net Co magnetic moment changes from negative to positive. In Figs. 3 and 4 it can be seen that at $T=135$ K and $\mu_0 H=2$ T for HoCo₂ and $T=35$ K and $\mu_0 H=1$ T for TmCo₂, the Co net magnetic moment is aligned parallel to the applied magnetic field, as expected in paramagnetism.

Up to this point, our results in R Co₂ for $R = \text{Dy, Ho, and Tm}$ show a behavior that is similar to that previously observed in ErCo₂¹. At higher temperatures, an interesting feature is found in these compounds. For example, the Dy signal in DyCo₂ is small, (indeed comparable to noise level) but the minute, positive signal at 1296 eV observable in the bottom right panel of Fig. 2 suggests a reversal on the sign of the Dy XMCD at the M₅ edge for $T > 228$ K. The Dy sublattice magnetization would become opposite to the Co net magnetization and to the applied magnetic field. The experimental results on HoCo₂ and TmCo₂ unambiguously confirm this trend: Ho and Tm M₅ XMCD signals change their sign at high temperature, above $T = 135$ K and $T = 35$ K, respectively (right bottom spectra of Fig. 3 and Fig. 4). In view of these results, two temperatures at which one of the two sublattice magnetization crosses zero well above the critical temperature can be defined: T_1 , where the net magnetization of Co changes from negative to positive and T_2 , where the net magnetization of the rare-earth sublattice changes from positive to negative (see Table I).

The separate thermal evolution of Ho and Co net magnetic moments obtained from XMCD measurements at $\mu_0 H=1$ T is shown in Fig. 6. The signals in the ferrimagnetic phase have been scaled to the values of Ho and the Co moments, as reported from neutron diffraction experiments.³⁸ As expected, the total magnetization measured in a SQUID magnetometer coincides with the sum of both magnetization sublattices, i.e., the sum of Ho and twice the Co net magnetization sublattices. Both Ho and Co magnetizations show abrupt jumps at the ordering transition. T_1 and T_2 are also indicated.

One would expect that under a sufficiently high applied magnetic field, the conventional paramagnetic configuration should be recovered. To complete our study of the paramagnetic phase of the R Co₂ series, we measured XMCD for applied fields from $\mu_0 H=0.25$ T up to $\mu_0 H=6$ T, at selected temperatures. Fig. 5 shows the XMCD spectra recorded at the Co L_{2,3} and Ho M_{4,5} edges (left and right panel, respectively) measured in HoCo₂ at $T=352$ K. The experimental results show that a field of $\mu_0 H=4$ T at room temperature is required to recover the polarization signs of conventional paramagnetism for HoCo₂. The Co XMCD signal is essentially unchanged, indicating that Co net magnetization is parallel to the applied magnetic field at $T=352$ K, independently of the orientations of the Ho net magnetic moment.

Four configurations, common to the three ferrimagnetic compounds for Co and R net magnetic moments are identified from the XMCD measurements under applied magnetic fields up to $\mu_0 H=5$ T in a temperature range between $T=4$ K to $T=350$ K : a) the long-range ordered antiparallel alignment below T_c ; b) the paramagnetic low-field intermediate-temperature phase, denoted as *paramagnetic-1*, (which is essentially the paramagnetism observed in ErCo₂); c) the expected high-temperature paramagnetic configuration, which almost disappears at low fields, substituted by d) an unexpected, high-temperature paramagnetic configuration with an inverted, negative net rare-earth magnetization, denoted as *paramagnetic-2* to differentiate it from the low temperature paramagnetic one.

B. ac magnetic susceptibility

As it has been discussed in previous works,^{1,9,39} the occurrence of paramagnetism in ErCo₂ is due to a competition of interactions on the Co sublattice. In particular, the Co-Co exchange interaction is responsible for the short-range order correlations which facilitate the collective reversal of the Co moments at the temperature where the net moment of the Co magnetic sublattice crosses zero. The phenomenology found by means of XMCD experiments in DyCo₂, HoCo₂, and TmCo₂, is similar to that observed in ErCo₂, and therefore short-range correlations in the paramagnetic phase of the R Co₂ systems considered in this study, are expected to occur. Indeed, previous SANS measurements have been used recently to probe the presence of short-range correlations within the magnetically disordered phase of HoCo₂,⁸ yielding a correlation length of 7 Å in HoCo₂ around T_1 , in coincidence with our previous result in ErCo₂¹. Magnetic ac susceptibility measurements will be presented here to get insight on the origin of paramagnetism in those compounds.

The inverse of $\chi'_{ac}(T)$, for DyCo₂ (left), HoCo₂ (center) and TmCo₂ (right), at selected applied magnetic fields between $\mu_0 H=0$ T to $\mu_0 H=5$ T is shown in Fig 7. In a standard paramagnetic system, the inverse of $\chi'_{ac}(T)$ has a linear dependence with temperature, according to the Curie-Weiss law

$$\chi'_{ac}(T) = \frac{C}{T - \theta} \quad \text{and} \quad C = \frac{N\mu_B^2}{3k_B} \mu_{eff}^2 \quad (1)$$

where N is the number of dynamic entities, θ is the Curie temperature, and μ_{eff} is the effective magnetic moment. R magnetic moments are two orders of magnitude larger than the Co one,^{40,41} for $T > T_c$ in the R Co₂, therefore, μ_{eff} is expected to be entirely due to the rare-earth moment.

Within this approximation, the dashed lines in Fig. 7 represent the contribution to the paramagnetic susceptibility from R ions by using the S, L and J values predicted by the Hund's rules, and assuming that only the ground state J is populated. The estimated values for

Compound	T_c (K)	XMCD		TS
		T_1 (K)	T_2 (K)	T_1 (K)
DyCo ₂	140	210 < T_1 < 228	228 < T_2 < 252	200
HoCo ₂	78	88 < T_1 < 112	135 < T_2 < 200	104
TmCo ₂	4.6	25 < T_1 < 32	38 < T_2 < 41	20

TABLE I. Temperatures T_1 (at which the net magnetization of Co changes from negative to positive) and T_2 (at which the net and magnetization of the rare-earth sublattice changes from positive to negative) estimated from XMCD and T_1 , obtained from TS measurements.

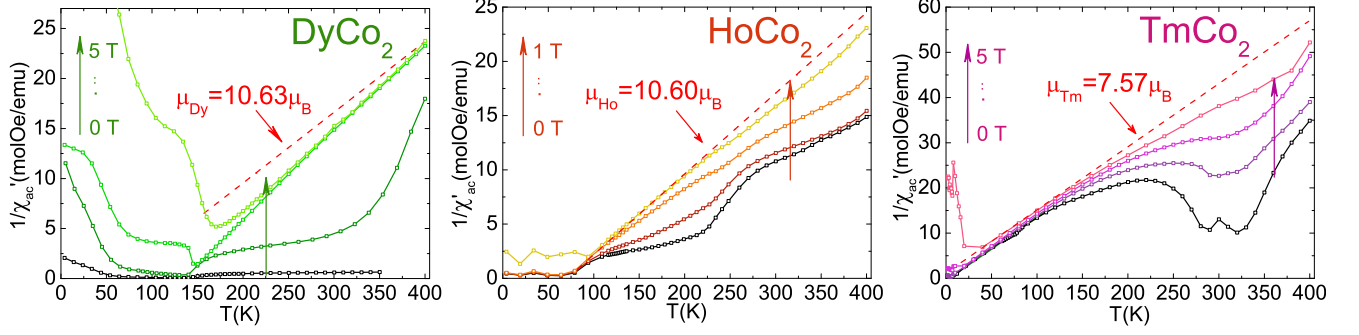


FIG. 7. (Color online) Temperature dependence of inverse of ac susceptibility. From left to right: DyCo₂; at $\mu_0 H = 0$ T, 0.04 T, 1 T and 5 T, HoCo₂; at $\mu_0 H = 0$ T, 0.05 T, 0.3 T and 1 T TmCo₂; at $\mu_0 H = 0$ T, 0.1 T, 1 T and 5 T. Dashed line shows the theoretical behavior expected for each system in the paramagnetic region according to Curie-Weiss law.

μ_{eff} are $10.63 \mu_B$, $10.60 \mu_B$ and $7.57 \mu_B$ for Dy, Ho and Tm ions, respectively. Clear deviations from those values and, in general, from a linear dependence with temperature of the χ_{ac}^{-1} can be observed for the three compounds, with the presence of one or two minima in the curves for $\mu_0 H \leq 1$ T. Those strong deviations from the simple Curie-Weiss curve at lower applied magnetic fields corresponds to values of μ_{eff} considerably higher than those estimated from the rare-earth magnetic moment only. For example, the curve measured at zero applied field for HoCo₂ allows to extract a Curie-Weiss value of $\mu_{eff} \sim 13 \mu_B$, about $2.5 \mu_B$ higher than the predicted value for R magnetic moment only. The high-temperature XMCD signal at the Co $L_{2,3}$ edges shows a non negligible magnetic moment in Co, that is nevertheless not large enough to explain the strong μ_{eff} observed. We ascribe the high value of μ_{eff} to the formation of volumes of short-length correlated spins, of about 1.5 nm in diameter near T_1 , as observed by SANS in ErCo₂ and HoCo₂^{1,8}.

At high applied fields, the ac magnetic susceptibility decreases and at $\mu_0 H = 5$ T the expected linear trend of the inverse susceptibility for RCo_2 with small, uncorrelated Co moments is almost recovered. This behavior, also observed in magnetically disordered ErCo₂, has been related with the *extreme sensitivity* to the applied field of χ_{ac} taking place at the onset of a Griffiths-like phase.^{19,23,25}

C. Radio-frequency transverse susceptibility and magnetic phase diagrams

Transverse Susceptibility (TS) technique has been used to study the anisotropic magnetic properties and magnetic switching in a variety of systems from multilayered thin films⁴² to single crystals⁴³ and nanoparticles.⁴⁴ More interesting to our case, a careful analysis of TS profiles (their shape and magnitude) has also revealed several fascinating features, such as phase coexistence and short-range correlations that are present in doped manganites^{43,45} and cobaltites.^{46,47} Indeed, the sensitivity of this technique to short-range magnetic correlations has been previously demonstrated in RCo_2 compounds^{10,11}, as it provides insight of the spin dynamics in each temperature region, particularly in their magnetically disordered phase. While an unipolar TS scan recorded below T_c , on a polycrystalline ferromagnet has a maximum at a field, H_M which coincides with the switching field, H_S , which is the field needed to reverse the direction of the net magnetization; an ideal paramagnet shows $H_M = 0$ ⁴⁵ since the magnetic moments are disordered and uncorrelated, being able to adiabatically follow the RF excitation. In contrast, the TS bipolar scans measured above T_c in ErCo₂ showed maxima at nonzero H_M in the temperature range where short-range magnetic correlations are present.¹⁰

In this work we present TS results performed in DyCo₂, HoCo₂ and TmCo₂. DyCo₂ bipolar scans are shown in

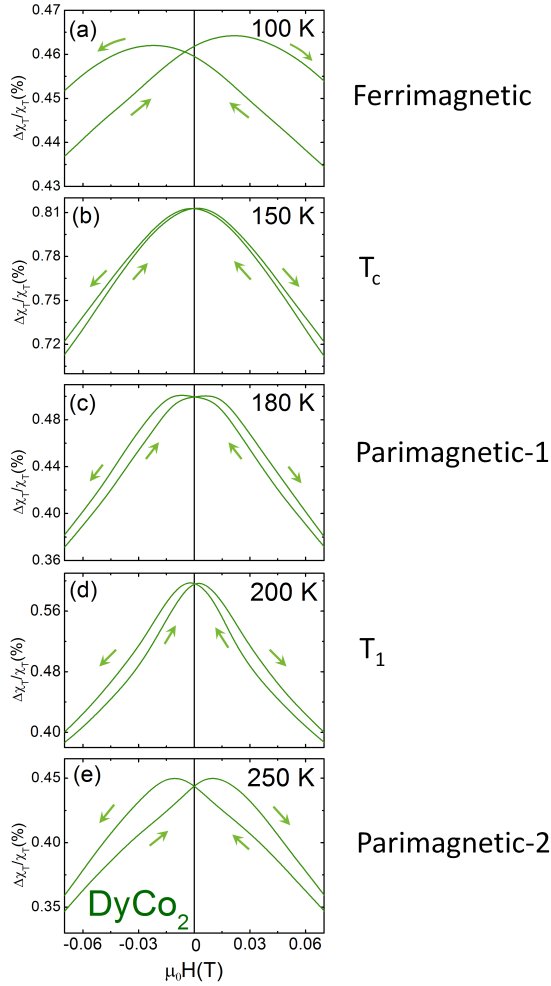


FIG. 8. (Color online) TS scans for DyCo₂, for $\mu_0 H_{sat} = 1$ T at selected temperatures representative of the TS profile evolution in ferri- (panel a), pari-1 (c) and pari-2 (e) phases; TS bipolar scans shown in panels (b) and (d) have been recorded at T_c and T_1 , respectively.

Fig. 8 for $\mu_0 H_{sat} = 1$ T at selected temperatures: $T=100$ K (panel a), 150 K (b), 180 K (c), 200 K (d) and 250 K (e), representative of the TS profile evolution in ferri- (panel a), pari-1 (c) and pari-2 (e) phases. TS bipolar scans shown in panels (b) and (d) have been recorded at T_c and T_1 , respectively. Panel (a) shows peaks at the switching field of ferrimagnetic DyCo₂. The peaks are broad, but the switching field can still be properly determined. TS bipolar scans at and above T_c are narrower than that measured below T_c . In particular, H_M is almost zero at T_c (panel b), but it is clearly nonzero at higher temperatures. The finite values of H_M found at $T > T_c$ in DyCo₂ suggest the occurrence of short-range correlations within the paramagnetic region. The short-range order gives rise to an increase in the field needed to reverse the magnetic moments, H_M , as they follow the RF excitation, in agreement with previous experimental works.^{10,43,46} A description for a similar study on HoCo₂

can be found in Ref. 8 where the same phenomenology has been observed up to temperatures as high as $T = 300$ K.

The temperature evolution of H_M can be obtained from the analysis of the TS profiles measured at a number of temperatures, as shown in the top panel of Figs. 9, 10, and 11 for DyCo₂, HoCo₂ and TmCo₂ respectively. In the three studied systems $H_M \neq 0$ for $T < T_c$ due to the long-range ferrimagnetic alignment between the *R* and Co magnetization sublattices. Then, the H_M profile shows a minimum at T_c , associated to the collective switching behavior of the rare-earth and Co moments in the ferrimagnetic ordered state. Above T_c , H_M never reaches zero in the measured temperature range. This is an indication of the presence of short-range correlations in all the *R*Co₂ compounds, since, as it has been pointed out before, $H_M = 0$ in an ideal paramagnet.

The H_M curve measured for DyCo₂ shows two minima, one at 150 K (at T_c) and a second one at $T=200$ K approximately coincident with T_1 as obtained from the XMCD analysis. The minima in the H_M profile matches with the maxima observed at the magnetic susceptibility, as it is shown in the middle panel of Fig. 9. At temperatures above T_1 , the H_M curve increases slowly, and no feature is present at the temperature T_2 due to the inversion of the Dy moments. These observations indicate that the net magnetic moment in the field direction due to the Co short-range correlated moments is the dominant contribution to the TS susceptibility for T above T_c . The *R* moments, instead, follow adiabatically the Co short-range correlated moments behavior. Magnetization measurements at temperatures above T_c have been performed in DyCo₂⁴⁸ corroborating that the H_M values depicted in Fig 9 within the disordered magnetic phase do not correspond to a switching field of any spurious ferro- or ferrimagnetic phase.

The characteristic relaxation time of the fluctuation due to these short-range correlations can be calculated from Ref. 9 as $\tau_{SRC} \simeq 10^{-3}$ s in the temperature range of T_1 which is much larger than the experimental time $\tau_{exp} = 1/\omega_{exp} = 10^{-7}$ s. Therefore, the maxima in the RF TS at $H \neq 0$ may be observed in spite of the paramagnetism shown by DC magnetization.⁴⁸ At $T > T_c$, the drag caused by this slow reaction to the RF excitation results in a displaced profile at each unipolar scan and the TS bipolar scans show two maxima, (at $\pm H_M$). As the Co net moment is reduced near the compensation temperature T_1 the τ_{SRC} decreases and therefore the value of H_M decreases. Similar results are found for HoCo₂ and TmCo₂, but additionally, in the case of HoCo₂ very large values of H_S can be also seen in the proximities of the spin reorientation transition that in this compound occurs at $T=16$ K.⁴⁹

The correspondence between the results from the TS and XMCD measurements can be seen more clearly when comparing the top panel of Figs. 9, 10, and 11 with their corresponding bottom panels, where new magnetic phase diagrams for DyCo₂, HoCo₂, and TmCo₂ are proposed

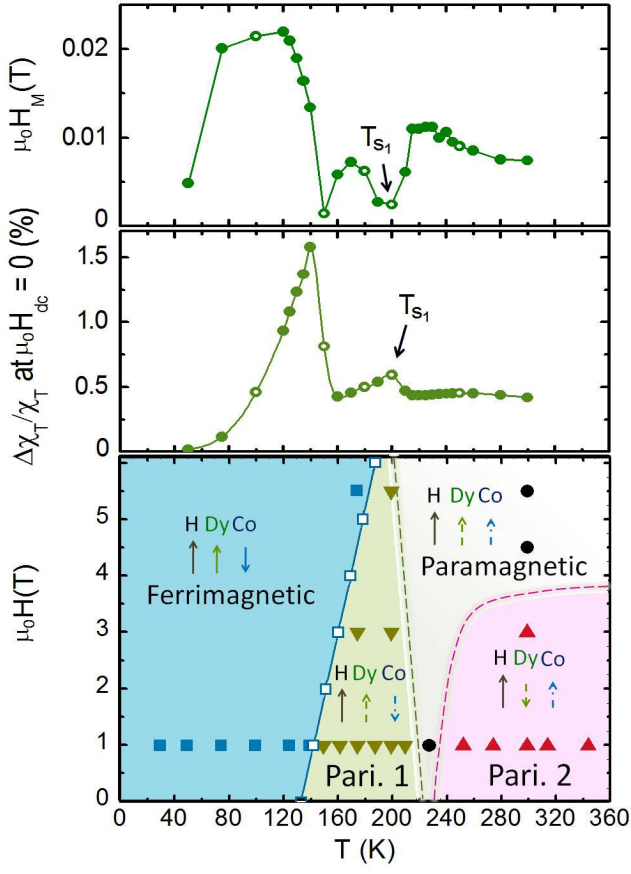


FIG. 9. (Color online) Top: Field at which a maxima is found in the TS unipolar scans $\mu_0 H_M$ as function of temperature for DyCo_2 . The values of H_M obtained from the selected temperatures in Fig. 8 are represented in open symbols. Middle: Susceptibility identified from TS measurements with $\mu_0 H^{sat} = 1$ T for DyCo_2 . Bottom: New magnetic phase diagram proposed for DyCo_2 from XMCD analysis for different fields and temperatures. Dashed line are a guide to the eye to separate the different configurations between the Co and Dy net magnetic moments. \square are selected values of T_c from the literature.⁴⁸ Full symbols indicate the field and temperature values at which XMCD measurements have been recorded in DyCo_2 . \blacksquare are used for the ferrimagnetic phase (Co \downarrow Dy \uparrow). ∇ , \bullet and \blacktriangle are used in the disordered region, to indicate the paramagnetic-1 (Co \downarrow Dy \uparrow), paramagnetic (Co \uparrow Dy \uparrow) and paramagnetic-2 configurations (Co \uparrow Dy \downarrow) respectively.

from our extensive XMCD data. In the magnetic phase diagrams, schemes of the magnetic configurations of Co and R moments are depicted to distinguish the ferrimagnetic, paramagnetic-1, paramagnetic and paramagnetic-2 configurations. The full symbols represent temperature and field values at which XMCD data were acquired to obtain the phase diagram. Square, inverted triangle, circle and triangle corresponds to the ferrimagnetic, paramagnetic-1, paramagnetic and paramagnetic-2 configurations respectively, as deduced from the Co $L_{2,3}$ and R $M_{4,5}$ XMCD spectra. Open squares are selected values

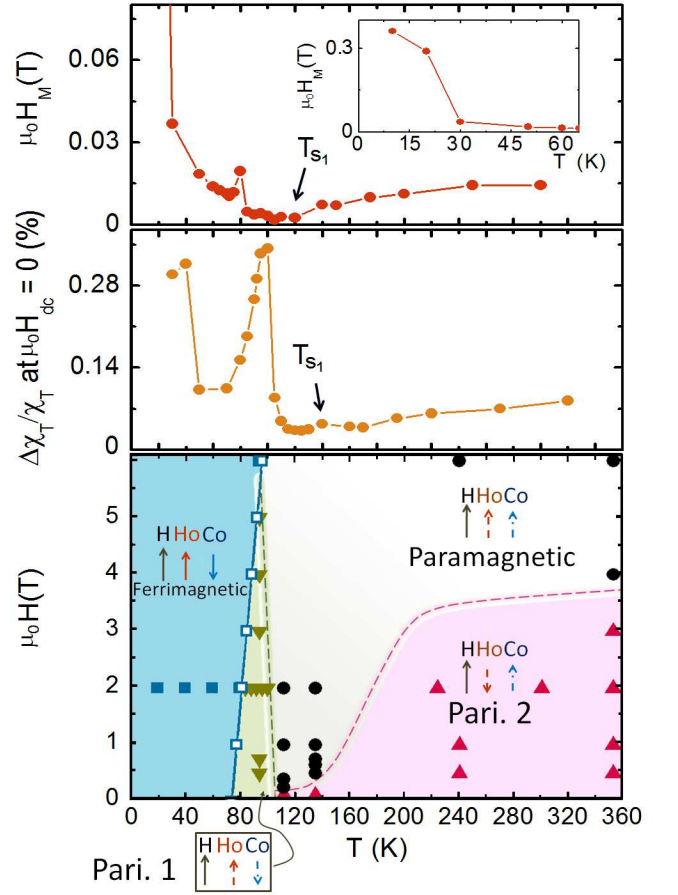


FIG. 10. (Color online) Top: Field at which a maxima is found in the TS unipolar scans $\mu_0 H_M$ as function of temperature for HoCo_2 . The inset shows the spin reorientation at low temperature in HoCo_2 that can be identified by a jump to very high H_M values at ~ 30 K. Middle: Susceptibility identified from TS measurements with $\mu_0 H^{sat} = 1$ T for HoCo_2 . Bottom: New magnetic phase diagram proposed for HoCo_2 from XMCD analysis for different fields and temperatures. Dashed line are a guide to the eye to separate the different configurations between the Co and Ho net magnetic moments. \square are selected values of T_c from the literature.⁴⁸ Full symbols indicate the field and temperature values at which XMCD measurements have been recorded in HoCo_2 . \blacksquare are used for the ferrimagnetic phase (Co \downarrow Ho \uparrow). ∇ , \bullet and \blacktriangle are used in the disordered region, to indicate the paramagnetic-1 (Co \downarrow Ho \uparrow), conventional paramagnetic (Co \uparrow Ho \uparrow) and paramagnetic-2 configurations (Co \uparrow Ho \downarrow) respectively.

of T_c obtained from the literature (Ref. 48). The dashed lines are a guide to the eye that suggest a separation between the regions at which the different alignments between the Co and R net magnetic moments take place on the magnetic phase diagram for $T > T_c$.

In general, the H_M curve depicts the same regions observed in the phase diagrams obtained from XMCD in the three compounds. However, the temperature T_1 obtained from TS measurements, is lower than the temperature T_1 obtained from XMCD in DyCo_2 and TmCo_2 .

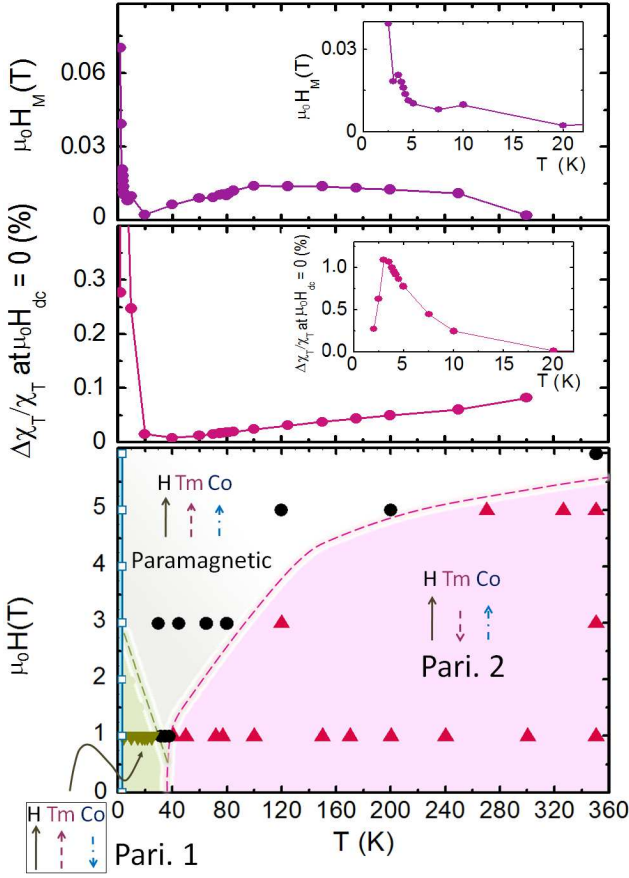


FIG. 11. (Color online) Top: Field at which a maxima is found in the TS unipolar scans $\mu_0 H_M$ as function of temperature for TmCo₂. The H_M and temperature ranges of the main panel and the inset of Fig. 11 have been chosen to allow the observation of the ordering transition at $T = 4.6$ K and the evolution of H_M for TmCo₂ above T_c . Middle: Susceptibility identified from TS measurements with $\mu_0 H^{sat} = 1$ T for TmCo₂. Bottom: New magnetic phase diagram proposed for TmCo₂. Dashed line are guides to the eye to separate the different configurations between the Co and Tm net magnetic moments. \square are values of T_c from magnetization as function of temperature measurements presented in Fig. 1. ∇ are the temperatures and fields at which the alignment between Co and Tm net magnetic moment is antiparallel for temperatures above T_c (parimagnetism-1). \bullet are the temperatures and fields at which the XMCD analysis indicates a parallel alignment between Co, Tm net magnetic moments and H (conventional paramagnetism). \blacktriangle are the temperatures and fields at which the XMCD analysis indicates that Tm net magnetic moment is antiparallel to Co net magnetic moment and to the applied field H (parimagnetism-2).

We ascribe such a discrepancy to the difference between the processes that are probed by each experiment; while XMCD is a static technique, TS is sensitive to the magnetic relaxation processes; therefore the temperature at which a given process is observed may vary. The XMCD experiments reflect R and Co magnetization separately

while the TS measurements senses the whole $R\text{Co}_2$ system. Table I allows to compare the compensation temperatures T_1 and T_2 obtained from XMCD at $\mu_0 H = 1$ T and the temperature T_1 obtained from TS experiments.

IV. DISCUSSION

The onset of parimagnetism can be understood as a result of the internal and external magnetic fields acting on the Co sublattice. Within the mean field approximation one can consider three contributions to the total field acting on one of the Co moments: the external applied field, H_{appl} , the molecular field due to the R sublattice, H_{R-Co} , and the molecular field from the Co sublattice itself, H_{Co-Co} . The direction of the applied magnetic field, H_{appl} defines the positive direction for magnetization. The magnitude of the molecular field for R and Co sublattices depends on both the total magnetization of each sublattice and the molecular field constants: n_{R-Co} , and n_{Co-Co} , which are proportional to the exchange interactions, J_{R-Co} , and J_{Co-Co} , respectively.

The key point to understand the $R\text{Co}_2$ magnetism above T_c lies in the fact that the Co-Co interaction ($J_{Co-Co} \sim 10$ meV)⁵ is much stronger than the Co- R interaction ($J_{R-Co} \sim 0.1$ meV).⁶ The difference of two orders of magnitude between the interactions would lead to a magnetism dominated by cobalt. However, the electronic structure is such that the Co magnetic moment in the paramagnetic region is about two orders of magnitude smaller than the rare-earth magnetic moments²⁸, and therefore, the interaction energies $J_{Co-Co}\mu_{Co}\mu_{Co}$ and $J_{R-Co}\mu_R\mu_{Co}$ are similar in magnitude. This equilibrium between the two internal fields may be easily destabilized by small or local variations on the crystal or electronic structure. J_{Co-Co} is so large that a fluctuation on the Co magnetic moment, either dynamic or static, will locally generate an exchange energy reduction by creating a short-range Co-Co ferromagnetically correlated zone. As cited before, the presence of magnetic short-range correlation have been confirmed by μSR spectroscopy in ErCo₂¹¹ below ~ 200 K, and short-range correlation lengths of about 8 Å below ~ 150 K have been evidenced by SANS^{1,8} in ErCo₂ and HoCo₂.

Moreover, the ac magnetic susceptibility in the paramagnetic region of $R\text{Co}_2$ ($R = \text{Ho}, \text{Dy}, \text{or Tm}$) at zero field clearly does not follow the expected Curie linear dependence. The actual curve obtained by measuring a given sample is batch- and history dependent, although the general tendency in polycrystalline samples is the one shown in Fig. 7: samples have a much larger polarizability than expected in the paramagnetic region, with susceptibilities typically two to five times larger than expected. The application of a (rather large) magnetic field is required to remove this extra polarizability and in some cases, $\mu_0 H = 5$ T are barely enough to recover the paramagnetic values. A very detailed characterization of the samples (x-ray and neutron diffraction, electron mi-

croscopy) do not show a noticeable presence of impurities which may reasonably explain the experimental behavior. However, any local deviation of stoichiometry would generate electronic and structural changes able to strongly correlate Co moments.

Indeed, density functional theory calculations to be published elsewhere⁵⁰ show that the formation of small Co short-range-correlations is favored near defects, vacancies, grain boundaries or electronic instabilities. This result reminds the strong spin fluctuations⁵¹ which have been relevant to understand the paramagnetism and the transport properties of the Co Laves phases for decades. Any instability that locally enhances a Co magnetic moment generates a very strong internal $H_{\text{Co-Co}}$ field, which easily may overcome the effect of the applied and $H_{\text{R-Co}}$ fields, enhancing short-range correlations around it. A very interesting novelty in this work is that, in RCo_2 , the Co short-range correlations not only generate paramagnetism at low field and temperature but also are able to reverse the (small) net magnetization of the rare earth sub-lattice at higher temperatures under moderate applied fields. Therefore, as long as short-range magnetic correlations are present; both configurations, paramagnetism-1 and paramagnetism-2, are explained by the competition between external and molecular fields acting on the Co moments.

As discussed in the Introduction, a Griffiths-like phase was identified in ErCo_2 ⁹. From the analysis of the longitudinal ac susceptibility, we find in DyCo_2 , HoCo_2 , and TmCo_2 the usual enhanced polarizability related with Griffiths phases, while the expected value is recovered under applied magnetic field.^{19,20,22,24} This sensitivity to the applied field is also characteristic of the formation of Griffiths phases.^{23,25} The enhanced effective moment values found in the magnetically disordered phase can be ascribed to the formation of spin-correlated volumes which are in agreement with previous SANS results^{1,8}, as expected in a Griffiths phase. Finally, the occurrence of paramagnetism itself requires that Co sublattice magnetization overcomes the lanthanide one, which is only possible if a relatively large number of Co moments ferromagnetically coupled form a larger, although short lived^{1,11}, cooperative magnetic moment. Therefore, it is plausible to propose the formation of a Griffiths-like phase above T_c in the RCo_2 compounds analyzed in this paper.

However, as also mentioned in the Introduction, a Griffiths phase occurs in a magnetic diluted system and it is observed through the formation of short-range magnetic correlations in the range $T_c < T < T_G$, being $T_G < T'_c$, the critical temperature of the undiluted system.

It is relevant to note that amorphous RCo_2 order magnetically at T_c^{am} well above room temperature (for example, ErCo_2 orders at $T_c^{\text{am}} \sim 500 \text{ K}$ ⁵² and $T_c^{\text{am}} > 400 \text{ K}$ for amorphous TbCo_2 ⁵³) Cobalt in amorphous ErCo_2 has a non negligible magnetic moment, and $J_{\text{Co-Co}} \mu_{\text{Co}} \mu_{\text{Co}}$ sets the magnetic order so that $T_c^{\text{am}} \approx 15 \cdot T_c^{\text{cryst}}$. In contrast, Co in crystalline RCo_2 has a reduced magnetic moment, as a consequence of the electronic structure in the or-

dered solid.⁷ One may think of the crystalline RCo_2 as a system in which magnetic Co has been “diluted” by the effect of the electronic structure. Therefore, RCo_2 could be considered as behaving like a magnetically “diluted” system, where the large cobalt moments, present in the amorphous phase, have been removed, indeed substituted by small, fluctuating magnetic moments (of the order of $0.2\mu_B$ in ErCo_2).²⁸ However, the Co-Co interaction is very strong ($J_{\text{Co-Co}} \sim 10 \text{ meV}$)⁵ and it comes naturally that spin fluctuation on Co moments in RCo_2 easily induce ferromagnetically correlated volumes. As said before, Co develops a magnetic moment in RCo_2 near any imperfections or grain boundaries present in the system. These magnetic moments may add to intrinsic, dynamical spin fluctuations to generate a background density of short range order correlations. Those would be at the origin of the observed Griffiths-like phase behavior, and in some cases may be stable enough to induce paramagnetism, i.e. to reverse the net magnetic moment of the rare earth ions at temperatures above room temperature, in a magnetically disordered image of the compensated state above $T_{\text{comp}}^{\text{am}}$.

In summary, paramagnetism would be a consequence of a Griffiths-like phase of the undiluted, high-temperature magnetically ordered amorphous RCo_2 . The new “dilution” mechanism at play in this Griffiths phase is not compositional, but purely magnetic, with origin in a combination of electronic-structure and local order around Co atoms. Considering the RCo_2 amorphous alloy as the “pure”, undiluted system sets T'_c clearly above room temperature. Moreover, amorphous ErCo_2 also shows a compensation point at about $T_{\text{comp}}^{\text{am}} \sim 230 \text{ K}$ ⁵²: above $T_{\text{comp}}^{\text{am}}$, Co net magnetization is larger than the Er one, whereas the opposite is true below $T_{\text{comp}}^{\text{am}}$. This phenomenology closely resembles what has been found in RCo_2 (for $R = \text{Dy}$, Ho , and Tm), giving raise to the paramagnetic-2 configuration.

V. CONCLUSIONS

Several experimental techniques have shown the existence of paramagnetism (the antiparallel configuration of the net magnetization of two sublattices within the paramagnetic phase) among ferrimagnetic systems in the Co Laves phases family. XMCD results in RCo_2 ($R = \text{Dy}$, Ho , and Tm) show not only the inversion of Co magnetization sublattice at a compensation temperature T_1 well above T_c , as observed in ErCo_2 . Surprisingly, the inversion of R magnetization sublattice at a second compensation temperature, $T_2 > T_1$, gives rise to a high temperature paramagnetic configuration, with the rare earth moment antiparallel to the Co one and to the field, which resembles the high temperature state of the magnetically ordered amorphous RCo_2 .

These findings depict a new magnetic phase diagram for DyCo_2 , HoCo_2 and TmCo_2 , with two new paramagnetic configurations above T_c and below an applied field

threshold of about 3 – 5 T. The origin of paramagnetism is understood in $R\text{Co}_2$ as a consequence of the relative intensity of both, the exchange interactions present in the system, and the relative magnitude of the cobalt and rare-earth magnetic moments. As the Co-Co exchange constant is two orders of magnitude stronger than the Co- R one, the molecular field of Co sublattice is dominant as soon as any fluctuation locally drives the Co magnetic moment higher than its average value, given by the electronic structure: a local deviation of stoichiometry, impurities, vacancies, or even statistical spin fluctuations would generate strong correlations between Co moments, originating the formation of short-range correlated volumes. The strength of the Co-Co interaction would transmit this correlations along the system. Indeed, the detailed study of TS profiles as function of temperature has shown a finite value of H_M for all temperatures and compounds, which is a clear indication of short-range correlations. On the other hand χ_{ac} measurements confirm a very high effective moment μ_{eff} , cal-

culated from the $\chi_{ac}^{-1}(T)$ curves, which is congruent with the occurrence of Co short-range correlations. The recovery of the Curie behavior under applied field suggest a Griffiths-like behavior, which has also been observed in ErCo_2 . An interpretation of paramagnetic $R\text{Co}_2$ as a Griffiths phase stands on an electronic structure - based dilution of the Co moment with respect to the “high temperature phase” represented by magnetically ordered amorphous $R\text{Co}_2$.

VI. ACKNOWLEDGMENTS

The financial support of MAT2011/23791, Aragones IMANA (partially funded by the European Social Fund) and the European FEDER funds is acknowledged. The authors acknowledge HZB for the allocation of synchrotron radiation beamtime. C. M. Bonilla acknowledge a Spanish MINECO grant and C. Castán and A. I. Figueroa acknowledge a JAE-Predoc CSIC grants.

-
- * mbonilla@unizar.es
- ¹ J. Herrero-Albillos, F. Bartolomé, L. M. García, A. Young, T. Funk, J. Campo, and G. J. Cuello, *Phys. Rev. B* **76**, 094409 (2007).
 - ² A. M. Stewart, *J. Phys. C: Solid State Phys.* **17**, 1557 (1984).
 - ³ D. Bloch and R. Lemaire, *Physical Review B* **2**, 2648 (1970).
 - ⁴ J. Déportes, D. Gignoux, and F. Givord, *Phys. Statu Solidi (b)* **64**, 29 (1974).
 - ⁵ J. J. Rhyne, *Journal of Magnetism and Magnetic Materials* **70**, 88 (1987).
 - ⁶ A. Castets, D. Gignoux, and B. Hennion, *Journal of Magnetism and Magnetic Materials* **15-18**, 375 (1980).
 - ⁷ E. Gratz, R. Resel, A. T. Burkov, E. Bauer, A. S. Markosyan, and A. Galatanu, *J. Phys.: Condens. Matter* **7**, 6687 (2001).
 - ⁸ C. M. Bonilla, I. Calvo, J. Herrero-Albillos, A. I. Figueroa, C. Castán-Guerrero, J. Bartolomé, J. A. Rodríguez-Velamazán, D. Schmitz, E. Weschke, D. Paudyal, V. K. Pecharsky, K. A. G. Jr, F. Bartolomé, and L. M. García, *Journal of Applied Physics* **111**, 07E315 (2012).
 - ⁹ J. Herrero-Albillos, L. M. García, and F. Bartolomé, *Journal of Physics: Condensed Matter* **21**, 216004 (2009).
 - ¹⁰ A. I. Figueroa, S. Chandra, M. H. Phan, H. Srikanth, C. M. Bonilla, F. B. L. M. García and, J. Bartolomé, and J. Herrero-Albillos, *Journal of Applied Physics* **109**, 07E118 (2011).
 - ¹¹ C. M. Bonilla, N. Marcano, J. Herrero-Albillos, A. Maisuradze, L. M. García, and F. Bartolomé, *Physical Review B* **84**, 184425 (2011).
 - ¹² A. Pirogov, A. Podlesnyak, T. Strassle, A. Mirmelstein, A. Teplykh, D. Morozov, and A. Yermakov, *Applied Physics A: Material Sciences Process* **74**, 598 (2002).
 - ¹³ A. Podlesnyak, T. Strassle, J. Schefer, A. Furrer, A. Mirmelstein, A. Pirogov, P. Markin, and N. Baranov, *Physical Review B* **66**, 012409 (2002).
 - ¹⁴ F. García, M. R. Soares, and A. Y. Takeuchi, *Journal of Magnetism and Magnetic Materials* **226-230**, 1197 (2001).
 - ¹⁵ M. R. Soares, A. Y. Takeuchi, F. García, S. F. da Cunha, and M. E. Massalami, *Journal of Magnetism and Magnetic Materials* **202**, 473 (1999).
 - ¹⁶ Y. Öner and O. Kamer, *Journal of Applied Physics* **103**, 07E137 (2008).
 - ¹⁷ J. Déportes, D. Givord, and K. R. A. Ziebeck, *Journal of applied physics* **52**, 2074 (1981).
 - ¹⁸ R. B. Griffiths, *Phys. Rev. Lett.* **23**, 17 (1969).
 - ¹⁹ Z. W. Ouyang, V. K. Pecharsky, K. A. G. Jr., D. L. Schlager, and T. A. Lograsso, *Physical Review B* **74**, 094404 (2006).
 - ²⁰ C. Magen, P. A. Algarabel, L. Morellón, J. P. Araújo, C. Ritter, M. R. Ibarra, A. M. Pereira, and J. B. Sousa, *Physical Review Letters* **96**, 167201 (2006).
 - ²¹ A. M. Pereira, L. Morellón, C. Magen, J. Ventura, P. A. Algarabel, M. R. Ibarra, J. B. Sousa, and J. P. Araújo, *Physical Review B* **82**, 172406 (2010).
 - ²² N. Pérez, F. Casanova, F. Bartolomé, L. M. García, A. Labarta, and X. Batlle, *Physical Review B* **83**, 184411 (2011).
 - ²³ M. Salamon and S. Chun, *Physical Review B* **68**, 014411 (2003).
 - ²⁴ M. Salamon, P. Lin, and S. Chun, *Physical Review Letters* **88**, 197203 (2002).
 - ²⁵ W. Jiang, X. Z. Zhou, G. Williams, Y. Mukovskii, and K. Glazyrin, *Physical Review B* **76**, 092404 (2007).
 - ²⁶ A. H. C. N. G. Castilla and B. A. Jones, *Physical Review Letters* **81**, 35313534 (1998).
 - ²⁷ Y. Öner and M. Guillot, *Journal of Magnetism and Magnetic Materials* **324**, 3313 (2012).
 - ²⁸ J. Herrero-Albillos, L. M. García, F. Bartolomé, A. Young, and T. Funk, *Journal of Magnetism and Magnetic Materials* **316**, e442 (2007).
 - ²⁹ F. Bartolomé, J. Herrero-Albillos, L. M. García, A. Young, T. Funk, N. Plugaru, and E. Arenholz, *Journal of Mag-*

- netism and Magnetic Materials **272**, 319 (2004).
- ³⁰ J. Herrero-Albillos, F. Bartolomé, L. M. García, J. Campo, A. Young, T. Funk, and G. J. Cuello., Journal of Magnetism and Magnetic Materials **310**, 1645 (2007).
 - ³¹ M. Mířek, J. Prokležka, V. Sechovský, D. Turcinková, J. Prchal, A. F. Kusmartseva, K. V. Kamenev, and J. Kamarád, Journal of Applied Physics **111**, 07E132 (2012).
 - ³² S. Khmelevskiy and P. Mohn., Journal of Physics: Condensed Matter **12**, 9453 (2000).
 - ³³ A. I. Figueroa, J. Bartolomé, J. M. G. del Pozo, A. Arauzo, E. Guerrero, P. Téllez, F. Bartolomé, and L. M. García, J. Magn. Magn. Mat. **324**, 2669 (2012).
 - ³⁴ C. T. Chen, Y. U. Idzerda, H. J. Lin, N. V. Smith, G. Meigs, E. Chaban, G. H. Ho, E. Pellegrin, and F. Sette, Physical Review Letters **75**, 152 (1995).
 - ³⁵ J. B. Goedkoop, *Ph. D. thesis* (Katolieke Universiteit te Nijmegen, 1989).
 - ³⁶ B. T. Thole and G. van der Laan, Europhysics Letters **4**, 1083 (1987).
 - ³⁷ S. Pizzini, L. M. García, A. Fontaine, J. P. Rueff, J. Vogel, R. M. Galera, J. B. Goedkoop, N. B. Brookes, G. Krill, and J. P. Kappler, Journal of Electron Spectroscopy and Related Phenomena **86**, 165 (1997).
 - ³⁸ D. Bloch and J. Voiron, Solid State Communications **12**, 685 (1973).
 - ³⁹ J. Herrero-Albillos, *Ph. D. Tesis Aplicación de nuevas sondas microscópicas al estudio del magnetismo de las fases de Laves RCo₂* (Universidad de Zaragoza, 2007) Chap. 7, pp. 168–174.
 - ⁴⁰ D. Gignoux, F. Givord, and J. Schweizer, Journal of Physics F: Metal Physics **7**, 1823 (1977).
 - ⁴¹ D. Gignoux, D. Givord, F. Givord, W. C. Koehler, and R. M. Moon, Phys. Rev. B **14**, 162 (1976).
 - ⁴² N. A. Frey, S. Srinath, H. Srikanth, M. Varela, S. Pennycook, G. X. Miao, and A. Gupta, Physical Review B **74**, 024420 (2006).
 - ⁴³ G. T. Woods, P. Poddar, H. Srikanth, and Y. M. Mukovskii, J. Appl. Phys. **97**, 10C104 (2005).
 - ⁴⁴ P. Poddar, M. B. Morales, N. A. Frey, S. A. Morrison, E. E. Carpenter, and H. Srikanth, Journal of Applied Physics **104**, 063901 (2008).
 - ⁴⁵ S. Chandra, A. I. Figueroa, B. Ghosh, M. H. Phan, H. Srikanth, and A. K. Raychaudhuri., Journal of Applied Physics **109**, 07D720 (2011).
 - ⁴⁶ C. Leighton, D. D. Stauffer, Q. Huang, Y. Ren, S. El-Khatib, M. A. Torija, J. Wu, J. W. Lynn, L. Wang, N. A. Frey, H. Srikanth, J. E. Davies, K. Liu, and J. F. Mitchell, Physical Review B **79**, 214420 (2009).
 - ⁴⁷ N. A. Frey Huls, N. S. Bingham, M. H. Phan, H. Srikanth, D. D. Stauffer, and C. Leighton, Phys. Rev. B **83**, 024406 (2011).
 - ⁴⁸ J. Herrero-Albillos, L. M. García, F. Bartolomé, F. Casanova, A. Labarta, and X. Batlle, Phys. Rev. B **73**, 134410 (2006).
 - ⁴⁹ F. G. D. Gignoux and R. Lemaire., Physical Review B **12**, 3878 (1975).
 - ⁵⁰ C. M. Bonilla and et al., In preparation.
 - ⁵¹ T. Nakama, K. Shintani, K. Yagasaki, A. T. Burkov, and Y. Uwatoko, Physical Review B **60**, 511D522 (1999).
 - ⁵² B. Boucher, A. Lienard, J. P. Rebouillat, and J. Schweizer., Journal of Physics F: Metal Physics **9**, 1421 (1979).
 - ⁵³ K. Buschow, *Handbook on Magnetic Materials, Magnetic Amorphous Alloys*, Amsterdam, Vol. 6 (Elsevier, Amsterdam, 1991) Chap. 4, p. 390.